Previous Article Next Article Articles ASAP Structure, Dynamics, and Spectral Diffusion of Water from First-Principles Molecular Dynamics

ARTICLE *in* THE JOURNAL OF PHYSICAL CHEMISTRY C · SEPTEMBER 2014

Impact Factor: 4.77 · DOI: 10.1021/jp506120t

THE JOURNAL OF PHYSICAL CHEMISTRY C

Article

pubs.acs.org/JPCC

Structure, Dynamics, and Spectral Diffusion of Water from First-Principles Molecular Dynamics

Arindam Bankura,[†] Anwesa Karmakar,[‡] Vincenzo Carnevale,* Amalendu Chandra,[‡] and Michael L. Klein*,[†]

[†]Institute for Computational Molecular Science and Department of Chemistry, Temple University, Philadelphia, Pennsylvania 19122, United States

[‡]Indian Institute of Technology, Kanpur 208016, India

Supporting Information

ABSTRACT: We have carried out first-principles Born−Oppenheimer molecular dynamics (BOMD) simulations of heavy water using density functional theory in conjunction with either empirical van der Waals (vdW) corrections or semilocal (van der Waals) exchange and correlation functionals. Specifically, gradient-corrected density functionals (BLYP), semiempirical vdW methods (BLYP-D2, BLYP-D3, PBE-D3, revPBE-D3), and vdW density functionals (DRSLL-PBE, DRSLL-optB88) are applied to evaluate their accuracy in describing the hydrogen-bonded network of heavy water. Ab initio trajectories are used to calculate structural and dynamical properties, with special emphasis on vibrational spectral diffusion and hydrogen bond dynamics. Our results show that inclusion of vdW interactions in DFT-GGA significantly affects the structure of liquid water and results in a faster diffusion. The combination of BLYP and revPBE functionals with the semiempirical vdW method of Grimme et al. [*J. Chem. Phys.* **2010**, *132*, 154104] and modified B88 functionals with the semilocal correlation functional according to M. Dion et al. [*Phys. Rev. Lett.* **2004**, *92*, 246401] provide the best agreement with experiments.

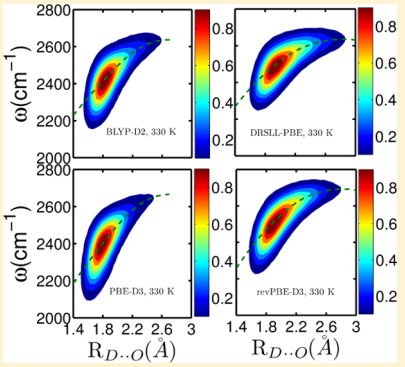

1. INTRODUCTION

Water is the most important liquid for life: the numerous cascades of biochemical events taking place in a cellular environment are ultimately governed by chemical reactivity in liquid water. Therefore, the structure, energetics, and dynamical properties of liquid water have been the object of extensive investigations.[1−3] Some properties of liquid water are unique, fascinating, and worth mentioning: the structure of water is characterized by a complex hydrogen bond (H-bond) network which leads to a very specific dependence of the density on the thermodynamic state, epitomized by the water density anomaly at T = 4 °C; the strong polarizability of liquid water, which is related to cooperative effects induced by H-bonding, determines its dielectric properties as well as the significant increase of the molecular dipole moment from 1.85 D in the gas to 2.9 ± 0.6 D in the liquid phase.[4−7]

So far ab initio molecular dynamics (MD) simulations of water have been performed mostly using the density functionals belonging to the category of generalized gradient approximation (GGA). This approximation is affected by the so-called self-interaction error that causes an excessive delocalization of the protons in H-bonds. Moreover, it neglects the nonlocal correlations responsible for vdW interactions. These interactions are weaker than H-bonds, but a number of recent works show that vdW interactions play a significant role in determining the structure of liquid water. As a result, density functional theory (DFT) within the generalized gradient approximation is known to poorly reproduce the experimental properties of liquid water. The poor description of the dispersion forces in the exchange correlation functionals is believed to be one of the possible causes. Recent studies have demonstrated an improvement in the simulated properties when the van der Waals (vdW) interactions are taken into account.

Using BLYP[8,9] and PBE[10] functionals at near-ambient conditions, the empirical dispersion correction referred to as DFT-D3[11,12] provides a more accurate description of the structure of liquid water.[13,14] Consistently, Jonchiere et al.[13] found that oxygen−oxygen radial distribution functions (RDFs) and diffusive properties of water are better described if the DFT-D3 correction is included when the triple-ζ valence doubly polarized (TZV2P) basis set is used in an NVT simulation at 322 K. However, recent investigations performed at different temperatures and/or at constant pressure have highlighted some of the limitations of this approach. Ma et al.[15] have shown that neither the BLYP nor the BLYP+D gives a satisfactory estimate of water density. They found that the density of water at 300 K and 1 bar is 1.07 and 0.92 g/cm^3, with and without dispersion, respectively. Thus, the error in the estimated density is of the same magnitude in both cases. Yoo

Special Issue: John C. Hemminger Festschrift

Received: June 19, 2014
Revised: September 5, 2014

   dx.doi.org/10.1021/jp506120t | *J. Phys. Chem. C* XXXX, XXX, XXX−XXX

et al.[16] used the same correction together with the BLYP functional in an NVT simulation at 385 K and found a severely understructured oxygen−oxygen RDF. Thus, for pure water, the improvement with the Grimme scheme is still far from perfect. The performance of the vdW functionals method can depend sensitively upon the choice of the exchange and correlation functional. Wang et al.[17] employed the PBE[10] and revPBE[19] functionals with the nonlocal vdW correlation functional proposed by M. Dion et al.[20] and obtained equilibrium densities for heavy water at 300 K and 1 bar of 1.13 and 1.02 g/cm^3, respectively. The oxygen−oxygen RDF of the PBE-vdW water accurately reproduced experimental results, while revPBE-vdW water exhibits a much softer structure. More recently, Zhang et al.[21] have used PBE, revPBE, PW86,[22] and a reparametrized version of the B88[8] exchange functional (optB88[23]) with the vdW correlation functional for liquid water. They found that optB88 yields the best agreement with experimental RDFs.

Vibrational spectral diffusion[24−31] of liquid water has been drawing the interest of many experimental[32−38] and theoretical groups[30,31,39−41] in the past few years, thanks to the potential insight that this property can provide on the dynamics of water molecules. Experimental characterization of spectral diffusion requires approaches like ultrafast 2D-IR vibrational echo as well as polarization-selective IR pump−probe experiments which can probe the picosecond and subpicosecond time scales.[32,33,42−50] From various experimental studies[32,37,51−58] it has been found that H-bond dynamics of liquid water occurs in a similar time scale of vibrational spectral diffusion of OH/OD stretching frequency. Like for other strongly H-bonded systems, vibrational spectral diffusion in water is related to the dynamics of H-bonds. The latter occurs on two time scales: a fast (∼100 fs) and a slow one (∼1−2 ps).[59−63] According to previous experimental and theoretical studies it was found that the first time scale corresponds to the dynamics of an intact water−water H-bond and the second time scale corresponds to water−water H-bond breaking and formation. Most of the theoretical studies made in this case do not include dispersion interactions. Few recent theoretical studies have shown already that inclusion of dispersion interactions improves both structural and diffusive properties in addition to a more realistic value of the density in the liquid state.

In this study, we have investigated and compared the structure, dynamics, and spectral diffusion properties of liquid water using conventional DFT, empirical vdW corrected DFT-D3, and nonlocal vdW-DF methods. To do so, we have performed ab initio molecular dynamics simulations of liquid water using the BLYP,[8,9] BLYP-D2, BLYP-D3,[11,12] PBE-D3, revPBE-D3, DRSLL-PBE, and DRSLL-optB88[8,9] functionals.

Specifically, in order to characterize the spectral diffusion of OD stretching frequencies, we have calculated the frequency−frequency time correlation function and also performed the transient hole dynamics calculations. Additionally, we have calculated the joint probability function of OD stretching frequency and O−D—O−D bond distance for all cases. To relate the calculated spectroscopic observables to the microscopic dynamics, we have also calculated the continuous H-bond correlation function, the distribution of dipole moments, the diffusion coefficient, and the orientational relaxation of various molecular vectors. Structural properties have been analyzed by calculating the RDFs for different interacting atomic sites of water molecules. It is found that, among these seven functionals, BLYP, BLYP-D2, and PBE-D3 functionals produce slower dynamics of spectral diffusion, while BLYP-D3, revPBE-D3, DRSLL-PBE, and DRSLL-optB88 functionals produce faster dynamics. The latter results are comparable to each other, and they are in good agreement with available experimental results.

2. SYSTEM SETUP AND FREQUENCY CALCULATION

2.1. System Setup. All the ab initio molecular dynamics simulations were performed with the CP2K package.[64] In CP2K, the electronic structure is calculated using the QUICKSTEP method[65] which uses a hybrid Gaussian and plane waves (GPW) scheme for calculating the energies and forces on atoms. In this approach, the Kohn−Sham[66] (KS) orbitals are expanded in terms of Gaussian orbitals, while a plane wave basis is used for the electron density. Such a dual basis set approach, combined with advanced multigrid, sparse matrix, and screening techniques, enables one to achieve an efficient linear-scaling evaluation of the KS matrix.

A reference MD simulation has been performed with the BLYP exchange-correlation density functional. To investigate the influence of dispersion forces on the structure and dynamics of liquid water, we have performed additional MD simulations where the dispersion forces are taken into account with the Grimme DFT-D2 and DFT-D3 method. The combination of Grimme DFT-D3 with PBE and revPBE functional was also considered. We also used different types of nonlocal vdW correlation functional methods (vdW-DF[20]) to account for the vdW interactions. The performance of the nonlocal vdW density functional methods depends crucially on the choice of the exchange functional. Therefore, ab initio MD simulations based on nonlocal vdW have been carried out using two different forms for the energy functional for the nonlocal vdW density functional methods, in which the exchange-correlation energy is given by one of PBE and optB88 functionals (hereafter referred to as DRSLL-PBE, DRSLL-optB88).

We have used a triple-ζ valence doubly polarized basis set to get a good compromise between the accuracy and computational cost.[67] Core electrons have been treated by using Goedecker−Teter−Hutter pseudopotentials.[68,69] For the auxiliary basis set of plane waves, a 400 Ry density cutoff (320 Ry for DRSLL-PBE, DRSLL-optB88) is used together with the NN50 smoothing method implemented in QUICKSTEP. We have done simulations for 64 water molecules in cubic box of length 12.418 Å. All the systems were equilibrated for ∼10 ps in a canonical ensemble at constant temperature of 330 K using the Nosé−Hoover thermostats[70,71] for all nuclear degrees of freedom with a time constant of 100 fs and a time step of 0.5 fs. Then the BOMD simulations were carried out for all systems in the NVE ensemble for trajectory generation of approximately 40 ps with a time step 0.5 fs. In all the cases, the first 5 ps have not been considered in the analysis. Classical equations of motion have been integrated using a time step of 0.5 fs. To maintain such a high time step and reduce the importance of quantum nuclear effects, hydrogen was substituted with deuterium.

The frequencies of OD stretching modes have been calculated from the time-dependent trajectories by using the wavelet analysis of time series method.[72−74] The details of the wavelet analysis for calculations of OD stretch frequencies from ab initio trajectories are available in refs 30 and 31.

dx.doi.org/10.1021/jp506120t | J. Phys. Chem. C XXXX, XXX, XXX−XXX

3. RESULTS AND DISCUSSIONS

3.1. Structure and Dipole Moment for Different Schemes of Dispersion Corrections. Structural arrangements of water molecules have been characterized here using the oxygen−oxygen and oxygen−hydrogen radial distribution functions. We have calculated radial distribution functions for oxygen−oxygen and oxygen−hydrogen pair interactions from the different ab initio MD simulations (Figure 1 and Figure 2).

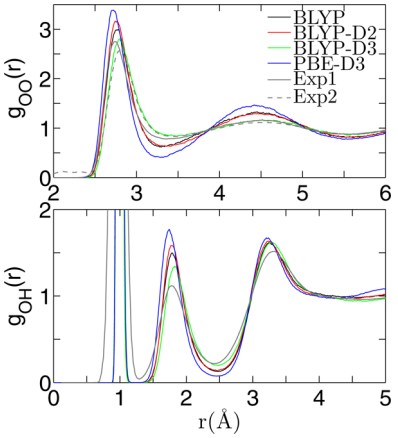

Figure 1. Radial distribution functions for oxygen−oxygen (upper panel) and oxygen−hydrogen (lower panel) correlations. The recent experimental oxygen−oxygen and oxygen−hydrogen RDFs, obtained from neutron scattering experiments (ref 75) and X-ray diffraction (ref 76), are shown as a solid and dashed gray line, respectively.

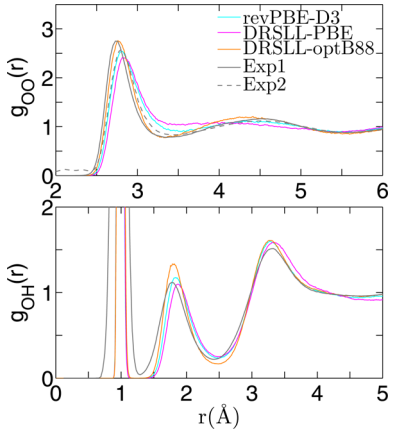

Figure 2. Radial distribution functions for oxygen−oxygen (upper panel) and oxygen−hydrogen (lower panel) correlations. The recent experimental oxygen−oxygen and oxygen−hydrogen RDFs, obtained from neutron scattering experiments (ref 75) and X-ray diffraction (ref 76), are shown as a solid and dashed gray line, respectively.

The numerical values for the height (h_{OO}^{max}) and the location of the first maxima (r_{OO}^{max}) and minima (r_{OO}^{min}) of the RDFs and the corresponding coordination numbers (n_{OO}) are given in Table 1. We have observed that the calculated coordination numbers (n_{OO}) are strongly dependent on the cutoff value chosen. We have calculated the coordination number using a cutoff value corresponding to the position of the first minimum (N_{OO}^{cord}) and a uniform cutoff value of 3.3 Å (N_{OO}^{cord}(3.3 Å)).

It is found that the BLYP, BLYP-D2, and PBE-D3 functionals actually overestimate the oxygen−oxygen pair correlation, displaying a stronger first peak and a much deeper first minimum with respect to both neutron scattering[75] and X-ray diffraction[76] data, whereas the peak heights of the oxygen−oxygen RDF of BLYP-D3, revPBE-D3, and DRSLL-optB88 functionals are very close to the experimental value.[75,76] The first maximum calculated from BLYP-D3 and revPBE-D3 simulations is at a distance about ∼0.1 Å larger than the neutron scattering[75] experimental results. The positions of the first minimum and the second maximum are in reasonably good agreement with those of the experimental oxygen−oxygen RDFs at 298 K. In particular, the oxygen−oxygen RDF from the revPBE-D3 simulation shows the best agreement with the X-ray diffraction[76] data, whereas the DRSLL-optB88 functional result is found to be very close to the neutron scattering result.[75] The PBE-D3 functional gives instead the oxygen−oxygen pair correlation function that deviates most from the experimental results. The peak height of the oxygen−oxygen RDF from DRSLL-PBE suggests a local structure that is softer than what is expected from experiments.

Addition of dispersion corrections (both DCACPs and DFT-D2) into the BLYP and revPBE functionals leads to a softer liquid structure. However, a dispersion-corrected PBE functional produces glass-like behavior. Our results are in fair agreement with these findings with similar oxygen−oxygen RDFs by Lin et al.[18] Results for the structural properties of water with the DRSLL-PBE functional have also been reported in ref 17. The agreement between those results and ours is only fair. We expect these differences to originate from the use of different basis sets and from the different simulation temperatures.

GGA functionals provide, in general, an inaccurate estimate of water density at constant pressure. Using an isobaric−isothermal (at room temperature and normal pressure) Monte Carlo simulation (NPT-MC), McGrath et al.[77] reported the structure and density of liquid water using the BLYP functional. Ben et al.[78] have used a similar NPT-MC framework and tested the performance of BLYP, BLYP-D3, PBE-D3, PBE0-ADMM-D3, and RI-MP2 for liquid water. Schmidt et al.[13] used isobaric−isothermal molecular dynamics (NPT-MD) simulations to investigate the influence of an empirical dispersion correction (Grimme DFT-D) on the exchange-correlation functional (BLYP and PBE). Ma et al.[15] have also reported the structure of water using NPT-MD for the BLYP and BLYP-D2 functionals. In all cases, GGA functionals like BLYP and PBE functionals gave a more structured and significantly less dense liquid (about 10−20%) than what is expected from the experiments. Inclusion of the dispersion correction significantly improves the oxygen−oxygen radial distribution function at the expense of an inaccurate prediction of the density, which turns out to be well above 1 g/cm^3. However, the reported peak heights of the oxygen−oxygen RDF (first shell) were different in the two schemes (NPT-MC and NPT-MD) despite the use of the same functional. For BLYP functionals, the average height of the first peak of the oxygen−oxygen RDF from NPT-MD is between 3.1 and 3.25, while the values from NPT-MC are in the 2.4−2.7 range.

The position and height of the peak of the oxygen−oxygen RDF from our BLYP, BLYP-D2, BLYP-D3, and PBE-D3 simulations is very similar to the NPT-MD and the NPT-MC simulations of Schmidt et al.,[13] Ma et al.,[15] and Ben et al.[78] Although the local structure is affected by the choice of the ensemble, the differences between different functionals are, in general, even larger.

dx.doi.org/10.1021/jp506120t | J. Phys. Chem. C XXXX, XXX, XXX−XXX

Table 1. Height of the RDF (h_{OO}^{max}) is Reported Together with the Positions (in Å) of the First Maximum (r_{OO}^{max}) and Minimum (r_{OO}^{min})[a]

	BLYP	BLYP-D2	BLYP-D3	PBE-D3	revPBE-D3	DRSLL-PBE	DRSLL-optB88	exptl
T	353	328	330	324	316	328	341	
h_{OO}^{max}	2.99	3.17	2.80	3.38	2.54	2.41	2.75	2.76,[75] 2.57[76]
r_{OO}^{max}	2.77	2.76	2.79	2.72	2.81	2.82	2.76	2.74,[75] 2.8[76]
r_{OO}^{min}	3.27	3.40	3.47	3.29	3.51	3.58	3.33	3.39,[75] 3.45[76]
N_{OO}^{cord}	4.1	4.6	5.1	4.1	5.3	5.7	4.3	4.6[75]
N_{OO}^{cord}(3.3 Å)	4.2	4.3	4.2	4.1	4.4	4.3	4.2	4.3[76]
N_{HB}	3.84	3.89	3.84	3.88	3.80	3.75	3.80	
μ	3.00	3.04	2.95	3.18	2.85	2.80	2.96	2.86[7]
τ^{HB}	2.28	2.46	1.15	5.0	0.97	0.76	1.43	0.5−1.7[59,60,62,63]
$\tau_1(\mu)$	13.93	7.02	3.67	41.5	2.43	2.52	3.50	
$\tau_2(\mu)$	6.16	2.89	1.23	19.64	0.97	0.83	1.40	1.7−2.5
τ_1(OH)	12.04	8.14	4.85	42.25	3.75	3.37	5.16	4.76[87]
τ_2(OH)	4.90	3.25	1.79	18.87	1.65	1.18	2.20	1.92[87]
D	1.14	0.71	1.81	0.39	1.85	2.57	1.57	1.87[85,86]

[a]Coordination numbers (n_{OO}^{cord}), number of hydrogen bonds per water molecule (N_{HB}), diffusion coefficient (D in 10^{-5} cm^2/s), dipole moments (μ in Debye), first ($\tau_1(\alpha)$) and second ($\tau_2(\alpha)$) order orientational relaxation time (in ps) along dipole and OH vector, and hydrogen bond dynamics (τ^{HB} in ps) are also reported.

In order to understand and quantify the effects of different functionals and dispersion corrections on the microscopic structure of liquid water, we have calculated the partial RDFs for each water molecule populating the first and second solvation shells. Specifically, at each molecular dynamics configuration, the nearest neighbors of each water molecule were ordered according to their distances. By averaging over all configurations and water molecules, the oxygen−oxygen RDFs for the nth neighbor were calculated. The partial RDFs of water for the 4th and 5th neighboring water molecules are shown in Figure 3. It is apparent that the average distance of the 4th and

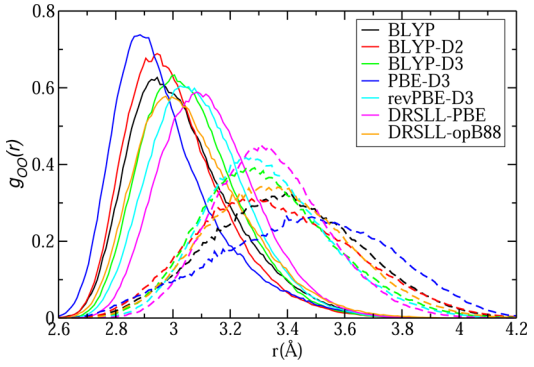

Figure 3. Partial oxygen−oxygen radial distribution functions for the fifth (solid line) and sixth (dashed line) neighboring water molecules obtained from ab initio molecular dynamics simulations using different functionals.

5th neighboring molecules is different for different functionals. In BLYP-D3, revPBE-D3, DRSLL-optB88, and DRSLL-PBE, an apparent outward shift with decreasing intensity was observed for the 4th neighbor with respect to BLYP, BLYP-D2, and PBE-D3 which of course results in a less pronounced peak height of the overall RDF. On the other hand, we observe the exact opposite behavior for the 5th and 6th neighboring (not shown here) water molecules which tend to simultaneously be shifted to smaller distances and increase the intensity of their contribution to the overall RDF. Due to the increase in the population of water molecules located in the interstitial region, i.e., the region between the first and second coordination shells, a significant reduction in the strength of the hydrogen bonds was observed with the use of dispersion correction to the exchange correlation functionals. Except the PBE-D3 and BLYP-D2, all other dispersion-corrected simulations indicate a deviation from the perfect tetrahedral hydrogen bonding network of ice and thus a softer structure of liquid water. Hence, we observed broader and less pronounced peaks in the oxygen−oxygen RDFs, a result in good agreement with the experimental data. However, this trend of destructuring or softening of the RDF was not observed for PBE-D3 and BLYP-D2.

We note that simply focusing on the RDFs is not enough to characterize the solvation structure of water, as angular correlations are also crucial. The structural differences of these simulations are characterized by examining the distribution of triplet oxygen−oxygen−oxygen (O−O−O) angles for the first coordination shells (shown in Figure 4). An experimental O−O−O angular distribution was recently extracted via empirical potential structural refinement (EPSR) based on joint X-ray/neutron scattering data. The experimental triplet O−O−O angular distribution shows a broad peak around 100°, indicating that the local tetrahedral network in liquid water is more disordered than in crystalline ice. The

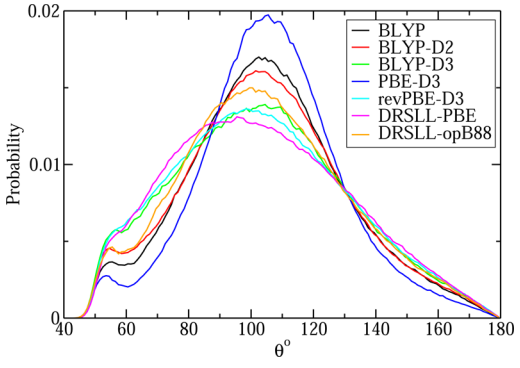

Figure 4. Distribution of triplet oxygen−oxygen−oxygen (O−O−O) angles for the first coordination shells obtained from ab initio molecular dynamics simulations using different functionals.

dx.doi.org/10.1021/jp506120t | J. Phys. Chem. C XXXX, XXX, XXX−XXX

triplet O−O−O angular distributions calculated from molecular dynamics trajectories show a significant change when the dispersion interactions are included in the simulations. The overall distribution was found to be different for different functionals; specifically, a broader and less pronounced distribution was observed for DRSLL-PBE, DRSLL-optB88, revPBE-D3, and BLYP-D3 functionals. The tetrahedral character of the first shell increases in this order: DRSLL-PBE, DRSLL-optB88, revPBE-D3, BLYP-D3, BLYP-D2, BLYP, and PBE-D3. The tetrahedral order is significantly reduced by the use of an exchange correlation functional with nonlocal dispersion interactions.

The coordination numbers determined by integrating up to the first peak minimum of the RDF vary considerably among the different models, whereas integration up to the distance cutoff of 3.3 Å of the oxygen−oxygen RDF gives the coordination numbers between 4.1 and 4.4. This strong cutoff dependence demonstrates the care needed when defining the O−O coordination in water. We have investigated the statistics of H-bonds for the water molecules by calculating the average number of accepted and donated H-bonds. There have been various widely adopted criteria to define hydrogen bonds based on interatomic distances and angles. We used a set of geometric criteria to define a H-bond. Two molecules are considered to be H-bonded if the distance (R_{OO}) between the oxygens of these molecules is smaller than 3.5 Å and the distance (R_{OH}) between the oxygen of the acceptor molecule and the hydrogen of the donor is less than 2.45 Å. We have calculated the average number of H-bonds per water molecule from our simulations, and the results are included in Table 1.

The dipole moment of liquid water is one of the most fundamental properties affecting, for instance, the dielectric response to an applied field. In the gas phase, the dipole moment of the molecule has been measured with great accuracy: it is 1.855 D.[4,5] Experimental estimates for liquid water, based on X-ray form factors, yield a value of 2.9 ± 0.6 D.[6,7] The main advantage of ab initio molecular dynamics calculation is that it allows one to quantitatively describe the polarization of each water molecule. Our calculation of dipole moments is based on the maximally localized Wannier functions (MLWF).[79] We have found that the results obtained using the BLYP-D3, revPBE-D3, DRSLL-PBE, and DRSLL-optB88 functionals are closer to the experimental results. The probability distributions of dipole moments are shown in Figure 5, and the average values are depicted in Table 1.

3.2. Hydrogen Bond Dynamics, Orientational Relaxation, and Diffusion. We have calculated the H-bond dynamics, orientational relaxation, and diffusion of water molecules. We define two H-bond population variables, $h(t)$ and $H(t)$, where $h(t)$ is equal to one when a particular water−water pair is H-bonded at time t according to the adopted definition and zero otherwise and $H(t) = 1$, if a water−water pair remains H-bonded from $t = 0$ to time t and is zero otherwise. With the help of these population variables, we construct the continuous H-bond time correlation function $S_{HB}(t)$[80−84] which gives the probability that an initially hydrogen bonded pair remains hydrogen bonded all the time from $t = 0$ to t

$$S_{HB}(t) = \frac{\langle h(0)H(t)\rangle}{\langle h(0)^2\rangle} \quad (1)$$

It is found that the BLYP, BLYP-D2, and PBE-D3 functionals show slower H-bond dynamics compared to the BLYP-D3, revPBE-D3, DRSLL-PBE, and DRSLL-optB88 functionals (Figure 6). The average H-bond lifetimes, as obtained by integrating $S_{HB}(t)$, are included in Table 1. The experimental results for this relaxation time vary between 0.5 and 1.7 ps.[34,36,53,58]

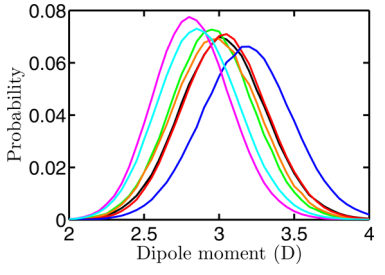

Figure 5. Dipole distribution of heavy water calculated from the NVE simulations (BLYP black, BLYP-D2 red, BLYP-D3 green, PBE-D3 blue, revPBE-D3 cyan, DRSLL-PBE pink, DRSLL-optB88 yellow).

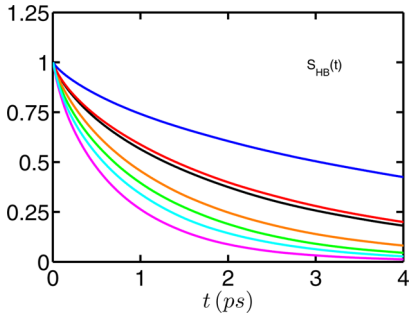

Figure 6. Time dependence of the continuous hydrogen bond time correlation functions calculated from the NVE simulations (BLYP black, BLYP-D2 red, BLYP-D3 green, PBE-D3 blue, revPBE-D3 cyan, DRSLL-PBE pink, DRSLL-optB88 yellow).

Rotational motion of water molecules is known to play a crucial role in the breaking of H-bonds. The rotational motion of water molecules is analyzed by calculating the orientational time-correlation function, $C_l^a(t)$, defined by

$$C_l^\alpha(t) = \frac{\langle P_l(e^\alpha(t)\cdot e^\alpha(0))\rangle}{\langle P_l(e^\alpha(0)\cdot e^\alpha(0))\rangle} \quad (2)$$

where P_l is the Legendre polynomial of rank l and e^a can be any vector joining two points on the water molecule. The results for the rotational relaxation of dipole and OD vectors are shown in Figures 7 and 8. We have calculated the rotational relaxation time for $l = 1$ and 2 and for the molecular dipole vector (μ) and along the O−D vectors (see Table 1). These orientational relaxation times were obtained by explicit integration of $C_l^a(t)$ from simulations until 10 ps at ambient condition and fitting the long-time decay by an exponential function. The orientational relaxation is also found to be slower for BLYP, BLYP-D2, and PBE-D3 functionals with respect to BLYP-D3, revPBE-D3, DRSLL-PBE, and DRSLL-optB88 functionals, and the trend which we have observed is very similar to spectral diffusion (discussed in the next section) and H-bond dynamics.

In order to investigate diffusion, we calculated the mean square displacement (MSD) of the water molecules. The MSD at long times is related to the diffusion coefficient (D) by the well-known Einstein relation

dx.doi.org/10.1021/jp506120t | J. Phys. Chem. C XXXX, XXX, XXX−XXX

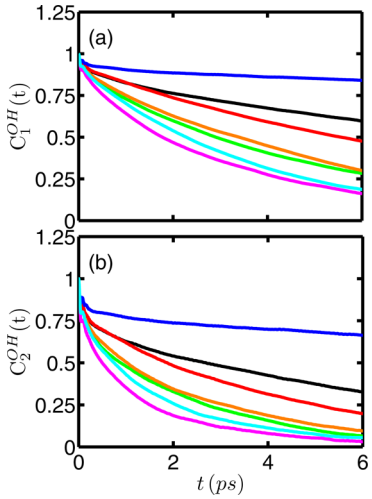

Figure 7. Time dependence of the first (upper panel) and second rank (lower panel) orientational correlation functions $C_l^a(t)$ for the rotation of OH vectors of heavy water molecules from the NVE simulations at the various levels of theory (BLYP black, BLYP-D2 red, BLYP-D3 green, PBE-D3 blue, revPBE-D3 cyan, DRSLL-PBE pink, DRSLL-optB88 yellow).

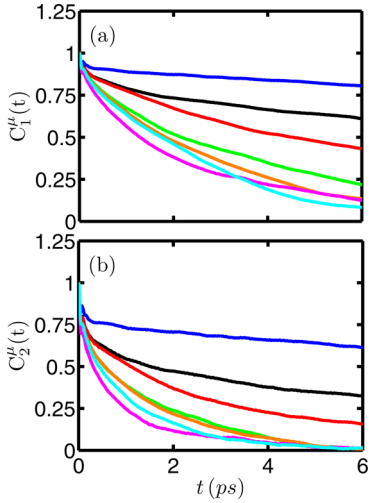

Figure 8. Time dependence of the first- (upper panel) and second-rank (lower panel) orientational correlation functions $C_l^a(t)$ for the rotation of dipole (μ) vectors of heavy water molecules from the NVE simulations (BLYP black, BLYP-D2 red, BLYP-D3 green, PBE-D3 blue, revPBE-D3 cyan, DRSLL-PBE pink, DRSLL-optB88 yellow).

$$D = \frac{1}{6}\lim_{t\to\infty}\frac{\langle |r(t) - r(0)|^2\rangle}{\Delta t} \tag{3}$$

where $r(t)$ is the position vector at time t. The values of the diffusion constants are obtained from the slope of a linear fit of the respective MSD data which we have calculated from our simulation trajectory. The MSD plots are shown in Figure 9, and the diffusion coefficient of water molecules calculated from different functionals have been reported in Table 1. We have found that the inclusion of dispersion interaction improves diffusional motion producing a diffusion coefficient which is in good agreement with the experimental results.[85,86]

3.3. Distribution of OD Stretching Frequency, Transient Hole Burning, and Frequency Correlation. The present study and also earlier studies[24−31,40,41,43] have shown that the time-dependent frequencies of OD modes are correlated with the length of the H-bond between the D atom and the nearest oxygen of a neighboring water. The time-dependent frequencies of the OD mode which is obtained from time series analysis are strongly correlated with the length of the H-bond between the D atom and the nearest oxygen of a neighboring water. It has been found that for a particular OD mode, when the D···O distance is large, the frequency of the OD mode is also found to be significantly higher than its average value. Here we have investigated how this relation holds for different functionals at ambient condition. In order to perform a detailed analysis on average, we have calculated the distribution of D···O distances for three fixed values of the OD frequency ($\delta\omega$ = 0 ± 5, 100 ± 5, and 100 ± 5 cm^{-1}, shown in Figure 10(a)) (also see Figure S-2(a)−Figure S-7(a) in the Supporting Information). The MATLAB package with 10−15% span in losses method for smoothing the raw simulation data

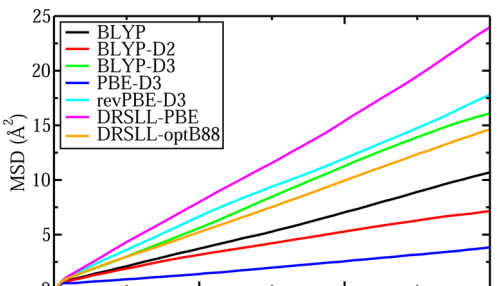

Figure 9. Mean square displacement (MSD) versus time for heavy water calculated from the NVE simulations (BLYP black, BLYP-D2 red, BLYP-D3 green, PBE-D3 blue, revPBE-D3 cyan, DRSLL-PBE pink, DRSLL-optB88 yellow).

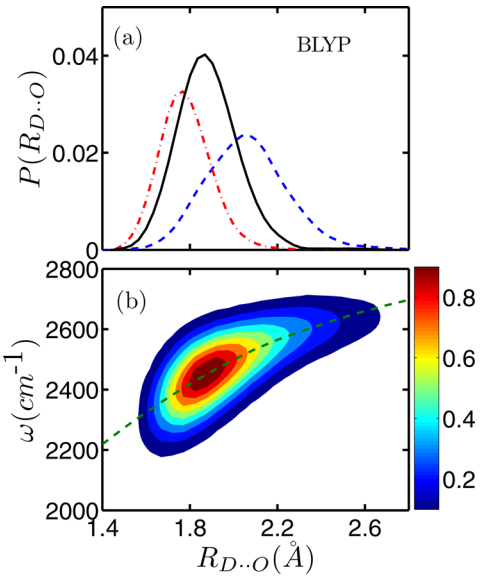

Figure 10. (a) Distribution of the D···O distance for fixed values of the OD frequency. The black solid, red dashed dotted, and blue dashed curves are for OD frequencies $\delta\omega$ = 0 ± 5, 100 ± 5, and 100 ± 5 cm^1, respectively, where $\delta\omega$ represents the deviation from the average frequency. (b) Joint probability distribution of the OD frequency and D···O distance. The contour levels of different fractions of the maximum value are shown in different color codes. The green dashed line (b) represents the monotonic relationship between the OD stretching frequency and hydrogen bond distance on average.

dx.doi.org/10.1021/jp506120t | J. Phys. Chem. C XXXX, XXX, XXX−XXX

was used for this plotting purpose. The relations are shown in Figure 10(b) (also see Figure S-1(a)−Figure S-7(b) in Supporting Information). It is seen that as the frequency increases, the corresponding distribution of D···O distances is also shifted toward its larger values. The wide distribution of frequency with significant overlaps does not allow to extract a single instantaneous frequency associated with a given D···O distance. When we calculated the joint probability function for OD stretching frequency and the associated H-bond distance, we observe a behavior similar to that shown previously for the distribution of water−water H-bond distances at three fixed values of OD stretching frequency.[30] We have not observed any significant changes in the qualitative results which establishes that a correlation between the OD stretching frequencies and D···O distances exist on average in liquid water (see Figure S-1 to Figure S-7 in the Supporting Information).

Our calculated average frequency of OD stretching modes for the BLYP, BLYP-D2, BLYP-D3, PBE-D3 revPBE-D3, DRSLL-PBE, and DRSLL-optB88 functionals are 2450.4, 2439.6, 2475.2, 2405.4, 2529.4, 2508.7, and 2458.9 cm^{-1}, respectively. For BLYP, the current value is slightly higher than the previously reported value since we have performed our simulations above 30 K of ambient temperature to avoid possible glassy behaviors.

The hole burning technique is a way of calculating the vibrational spectral diffusion of OD stretching modes.[24,25,30,31,39] In this case, a subset of OD stretching frequencies is excited from an equilibrium set of OD stretching frequencies, called hole modes, and the remaining modes of OD stretching frequencies are considered to be as inhomogeneous or nonequilibrium distribution of OD stretching frequency corresponding to their laser promotion. The time scale of spectral shift is directly correlated with the water−water H-bond distance. It is assumed that a laser pump pulse having Gaussian frequency profile burns a hole at $t = 0$ in the ground state frequency distribution of the form[24,25,30,31,39]

$$P_h(\omega, 0) = P_{eq}(\omega)e^{-(\omega-\omega_p)^2/2\sigma^2} \tag{4}$$

where ω_p is the pulse center frequency and P_{eq} denotes the equilibrium frequency distribution of the OD modes of interest. Clearly, the initial distribution of the remaining OD frequencies $P_r(\omega, 0)$, i.e., the ones remaining in the ground state in experimental situations, is equal to $P_{eq}(\omega) - P_h(\omega, 0)$. We use a Gaussian pulse of full width (2σ) of 140 cm^{-1} and calculate the time evolution of nonequilibrium distributions $P_r(\omega, t)$ and $P_h(\omega, t)$ from a large set of system trajectories reflecting the initial distributions $P_r(\omega, 0)$ and $P_h(\omega, 0)$, respectively. The average frequency of the hole modes at time t is then calculated from the following relation

$$\bar{\omega}_h(t) = \frac{1}{N_h}\int d\omega\omega P_h(\omega, t) \tag{5}$$

where $N_A = \int d\omega P_h(\omega, 0)$. The average time-dependent frequency of the remaining modes is calculated in a similar way. A subset of OD modes is chosen for hole dynamics calculation where the average frequency shifts of the hole modes of water molecules have been studied by creating holes in two different frequency regions: one centered in the red side at $\omega_p = \bar{\omega}_{hyd} - 100$ cm^{-1} and the other centered in the blue side at $\omega_p = \bar{\omega}_{hyd} + 100$ cm^{-1} where, as defined earlier, $\bar{\omega}_{hyd}$ is the average frequency of all the OD groups. A similar scheme is used here for the study of dynamics of remaining OD modes. Further details of the hole dynamics calculations are available elsewhere.[25,30,31]

We have shown (see Figure S-8−Figure S-14 in the Supporting Information) the time dependence of the average frequencies of the hole modes $(\Delta\bar{\omega}_h)$ for both blue and red excitations. The corresponding results for the remaining modes $(\Delta\bar{\omega}_r)$ are also shown (see Figure S-8−Figure S-14 in the Supporting Information) for the different simulations. The frequency is expressed in terms of the shift $(\Delta\omega)$ from the equilibrium value averaged over all the modes. It is found that there is a fast decay and an oscillation at short times followed by slower decay extending to a few picoseconds. A biexponential fit does not include the small oscillation present in the simulation results at short times. We have fitted our results by using a triexponential function with damped oscillation term[25,30,31]

$$f(t) = a_0\cos(\omega_S t)e^{-t/\tau_0} + a_1 e^{-t/\tau_1} + (1 - a_0 - a_1)e^{-t/\tau_2} \tag{6}$$

Calculation of frequency−frequency time correlation function provides another way to study the vibrational spectral diffusion. The frequency−frequency time correlation function is calculated using the relation

$$C_\omega(t) = \frac{\langle\delta\omega(t)\delta\omega(0)\rangle}{\langle\delta\omega(0)^2\rangle} \tag{7}$$

where $\delta\omega(t)$ is the fluctuation from the average frequency at time t. We have fitted our results using eq 6. The results are shown in Figure 11, and the corresponding time scales for spectral diffusion are given in Table 2. The short decay time (τ_0) scale arises from the underdamped motion of intact H-bonded O···O pairs. A separate calculation of the power spectra of the relative velocity of an initially H-bonded O···O pair is done to get the reason for this underdamped motion. Both bending and stretching modes of intermolecular vibrations can modulate the OD frequencies and hence contribute to the short-time oscillation of the frequency−time correlation function (see Figure S-15 in the Supporting Information). We have found from our study that BLYP, BLYP-D2, and PBE-D3 functionals produce slower dynamics with respect to the results of BLYP-D3, revPBE-D3, RSLL-PBE, and DRSLL-optB88 functionals. Our calculated results of spectral diffusion are in good agreement with the already available experimental results.

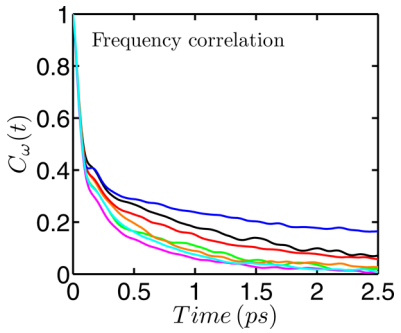

Figure 11. Time correlation function of OD fluctuating frequencies averaged over all of the molecules of the system from the NVE simulations (BLYP black, BLYP-D2 red, BLYP-D3 green, PBE-D3 blue, revPBE-D3 cyan, DRSLL-PBE pink, DRSLL-optB88 yellow).

dx.doi.org/10.1021/jp506120t | J. Phys. Chem. C XXXX, XXX, XXX−XXX

Table 2. Spectral Diffusion Data for All OD Modes from Various Methods Used in Our Simulation[a]

methods	quantity	excitation	τ_0	τ_1	τ_2	ω_s	a_0	a_1
BLYP	$C_\omega(t)$		0.10	0.12	1.74	130.24	0.20	0.48
	$\Delta\bar{\omega}_h(t)$	blue	0.12	0.11	1.64	104.61	0.25	0.44
	$\Delta\bar{\omega}_r(t)$	blue	0.14	0.10	2.42	109.04	0.17	0.45
	$\Delta\bar{\omega}_h(t)$	red	0.14	0.11	2.32	76.43	0.13	0.47
	$\Delta\bar{\omega}_r(t)$	red	0.12	0.11	1.46	76.43	0.17	0.52
BLYP-D2	$C_\omega(t)$		0.11	0.10	1.64	144.36	0.10	0.61
	$\Delta\bar{\omega}_h(t)$	blue	0.12	0.11	1.09	118.28	0.24	0.48
	$\Delta\bar{\omega}_r(t)$	blue	0.12	0.13	3.00	127.38	0.24	0.53
	$\Delta\bar{\omega}_h(t)$	red	0.17	0.13	2.16	118.21	0.14	0.55
	$\Delta\bar{\omega}_r(t)$	red	0.16	0.14	1.20	122.29	0.16	0.55
BLYP-D3	$C_\omega(t)$		0.12	0.10	0.93	128.50	0.15	0.57
	$\Delta\bar{\omega}_h(t)$	blue	0.12	0.12	0.88	112.76	0.14	0.64
	$\Delta\bar{\omega}_r(t)$	blue	0.16	0.14	1.53	115.87	0.12	0.64
	$\Delta\bar{\omega}_h(t)$	red	0.14	0.14	1.24	126.62	0.13	0.65
	$\Delta\bar{\omega}_r(t)$	red	0.13	0.15	1.16	126.11	0.16	0.74
PBE-D3	$C_\omega(t)$		0.08	0.15	4.55	129.20	0.29	0.42
	$\Delta\bar{\omega}_h(t)$	blue	0.14	0.10	5.63	117.19	0.19	0.64
	$\Delta\bar{\omega}_r(t)$	blue	0.13	0.11	7.08	122.29	0.19	0.58
	$\Delta\bar{\omega}_h(t)$	red	0.16	0.20	7.0	121.93	0.19	0.54
	$\Delta\bar{\omega}_r(t)$	red	0.16	0.13	4.16	122.29	0.19	0.56
revPBE-D3	$C_\omega(t)$		0.10	0.11	0.72	118.78	0.21	0.48
	$\Delta\bar{\omega}_h(t)$	blue	0.16	0.12	0.62	122.29	0.15	0.57
	$\Delta\bar{\omega}_r(t)$	blue	0.11	0.21	2.40	112.10	0.26	0.64
	$\Delta\bar{\omega}_h(t)$	red	0.12	0.18	1.48	112.10	0.19	0.62
	$\Delta\bar{\omega}_r(t)$	red	0.12	0.26	1.23	91.72	0.30	0.59
DRSLL-PBE	$C_\omega(t)$		0.10	0.11	0.76	117.56	0.19	0.57
	$\Delta\bar{\omega}_h(t)$	blue	0.18	0.12	0.55	117.20	0.11	0.58
	$\Delta\bar{\omega}_r(t)$	blue	0.18	0.14	0.90	117.20	0.12	0.68
	$\Delta\bar{\omega}_h(t)$	red	0.16	0.14	0.95	117.20	0.13	0.65
	$\Delta\bar{\omega}_r(t)$	red	0.17	0.11	0.55	117.20	0.11	0.53
DRSLL-optB88	$C_\omega(t)$		0.10	0.11	0.80	120.91	0.18	0.48
	$\Delta\bar{\omega}_h(t)$	blue	0.16	0.10	0.62	114.85	0.15	0.52
	$\Delta\bar{\omega}_r(t)$	blue	0.15	0.13	1.32	113.38	0.18	0.60
	$\Delta\bar{\omega}_h(t)$	red	0.17	0.17	1.20	106.07	0.17	0.62
	$\Delta\bar{\omega}_r(t)$	red	0.15	0.12	0.49	105.36	0.18	0.42

[a]The time constants (ps), frequency (cm^{-1}), and weights of the time-dependent frequency shifts of the hole and remaining modes for blue and red excitations of OD bonds.

4. CONCLUSIONS

Accurate modeling of water is crucial to get a good description of the hydrogen bond dynamics and thus of vibrational spectral diffusion. Here we have looked at the effects of dispersion interactions on hydrogen bond dynamics and vibrational spectral diffusion from the analysis of trajectories generated from ab initio molecular dynamics simulation using CP2K at a temperature slightly higher than room temperature (30 K higher). We have characterized quantitatively spectral diffusion of water molecules using both the transient hole burning technique and frequency−frequency time correlation function methods. We have found that for all cases the BLYP, BLYP-D2, and PBE-D3 functionals produce slower dynamics than that produced by other functionals. We observed a linear relation between the instantaneous OD stretching frequency and the corresponding hydrogen bond distance for all cases investigated. The analysis of hydrogen bond dynamics and orientational relaxation was done by constructing proper population correlation functions. We have found that the BLYP, BLYP-D2, and PBE-D3 functionals produce slower hydrogen bond dynamics and orientational relaxation with respect to others. When we have calculated the dipole moment of individual water molecules using the centers of the maximally localized Wannier functions, we have found that the dipole moment values resulting from BLYP-D3, revPBE-D3, DRSLL-PBE, and DRSLL-optB88 functionals are very close to the experimental results. Our results of diffusional motion of water molecules using the mean square displacement as a function of time show that inclusion of dispersion interactions significantly improves the agreement with the experimental results of the diffusion coefficient of bulk liquid water. Strikingly, BLYP-D3, revPBE-D3, DRSLL-PBE, and DRSLL-optB88 functionals give rise to similar dynamics of water molecules, though significant changes in oxygen−oxygen radial distribution functions are also found.

The diffusivity of the liquid water is much higher than that of ice due to the continuous breaking and formation of hydrogen bonds. In ice, each water molecule is connected to four water molecules. However, a fraction of the hydrogen bonds are broken in liquid water due to the effect of thermal motions. The spatial arrangement of neighboring water molecules has a direct impact on the dynamics and diffusion in the liquid phase. In this work we observed that the water molecules in the second solvation shell move inward and populate the interstitial

dx.doi.org/10.1021/jp506120t | J. Phys. Chem. C XXXX, XXX, XXX−XXX

region, when the dispersion interactions are included in the exchange correlation functionals. As a result, the hydrogen bonding in the first solvation shell is weakened, and a larger degree of disorder in the local tetrahedral network of liquid water is observed. As BLYP, BLYP-D2, and PBE-D3 predict a more pronounced tetrahedral hydrogen bonding network, we expect water molecules to be less diffusive and produce slower dynamics in these cases.

■ ASSOCIATED CONTENT

Supporting Information

Additional plots are provided. The plots show: frequency distributions of OD stretching modes for different values of hydrogen bond angle; distribution of the D···O distance for fixed values of the OD frequency; time variation of the average frequency shifts of the hole modes and remaining modes; and power spectra of O···O relative velocities of an initially. This material is available free of charge via the Internet at http://pubs.acs.org.

■ AUTHOR INFORMATION

Corresponding Authors

*E-mail: mlklein@temple.edu.

*E-mail: vincenzo.carnevale@temple.edu.

Notes

The authors declare no competing financial interest.

■ ACKNOWLEDGMENTS

This research used resources of the National Energy Research Scientific Computing Center, which is supported by the Office of Science of the U.S. Department of Energy under Contract No. DE-AC02-05CH11231. A.B. receives partial support from DOE BES Award No. DE FG-0212ER16333. A.K. and A.C. gratefully acknowledge the financial support from the Department of Science and Technology (DST) and Council of Scientific and Industrial Research, Government of India.

■ REFERENCES

(1) Franks, F., Ed. *Water a Comprehensive Treatise*; Plenum: New York, 1972; Vols. *1*−*4*.

(2) Head-Gordon, T.; Hura, G. Water Structure from Scattering Experiments and Simulation. *Chem. Rev. (Washington, D.C.)* **2002**, *102*, 2651−2670.

(3) Rey, R.; Møller, K. B.; Hynes, J. T. Ultrafast Vibrational Population Dynamics of Water and Related Systems: a Theoretical Perspective. *Chem. Rev. (Washington, D.C.)* **2004**, *104*, 1915−1928.

(4) Tu, Y. Q.; Laaksonen, A. the Electronic Properties of Water Molecules in Water Clusters and Liquid Water. *Chem. Phys. Lett.* **2000**, *329*, 283−288.

(5) Shostak, S. L.; Ebenstein, W. L.; Muenter, J. S. the Dipole Moment of Water. I. Dipole Moments and Hyperfine Properties of H_2O and HDO in the Ground and Excited Vibrational States. *J. Chem. Phys.* **1991**, *94*, 5875−5882.

(6) Coutinho, K.; Guedes, R. C.; Costa Cabral, B. J.; Canuto, S. Electronic Polarization of Liquid Water: Converged Monte Carlo-Quantum Mechanics Results for The Multipole Moments. *Chem. Phys. Lett.* **2003**, *369*, 345−353.

(7) Badyal, Y. S.; Saboungi, M.-L.; Price, D. L.; Shastri, S. D.; Haeffner, D. R.; Soper, A. K. Electron Distribution in Water. *J. Chem. Phys.* **2000**, *112*, 9206−9208.

(8) Becke, A. D. Density-Functional Exchange-Energy Approximation with Correct Asymptotic Behavior. *Phys. Rev. A* **1988**, *38*, 3098.

(9) Lee, C.; Yang, W.; Parr, R. G. Development of the Colle-Salvetti Correlation-Energy Formula into a Functional of the Electron Density. *Phys. Rev. B* **1988**, *37*, 785.

(10) Perdew, J. P.; Burke, K.; Ernzerhof, M. Generalized Gradient Approximation Made Simple. *Phys. Rev. Lett.* **1996**, *77*, 3865.

(11) Grimme, S. Semiempirical GGA-Type Density Functional Constructed with A Long-Range Dispersion Correction. *J. Comput. Chem.* **2006**, *27*, 1787−1799.

(12) Grimme, S.; Antony, J.; Ehrlich, S.; Kreig, H. a Consistent and Accurate Ab Initio Parametrization of Density Functional Dispersion Correction (DFT-D) for the 94 Elements H-Pu. *J. Chem. Phys.* **2010**, *132*, 154104.

(13) Schmidt, J.; Vande Vondele, J.; Kuo, I.-F. W.; Sebastiani, D.; Siepmann, J. I.; Hutter, J.; Mundy, C. J. Isobaric- Isothermal Molecular Dynamics Simulations Utilizing Density Functional Theory: an Assessment of the Structure and Density of Water At Near-Ambient Conditions. *J. Phys. Chem. B* **2009**, *113*, 11959−11964.

(14) Jonchiere, R.; Seitsonen, A. P.; Ferlat, G.; Saitta, A. M.; Vuilleumier, R. Van Der Waals Effects in Ab Initio Water At Ambient and Supercritical Conditions. *J. Chem. Phys.* **2011**, *135*, 154503.

(15) Ma, Z.; Zhang, Y.; Tuckerman, M. E. Ab Initio Molecular Dynamics Study of Water At Constant Pressure Using Converged Basis Sets and Empirical Dispersion Corrections. *J. Chem. Phys.* **2012**, *137*, 044506.

(16) Yoo, S.; Xantheas, S. S. Communication: the Effect of Dispersion Corrections On the Melting Temperature of Liquid Water. *J. Chem. Phys.* **2011**, *134*, 121105.

(17) Wang, J.; Román-Pérez, G.; Soler, J. M.; Artacho, E.; Fernández-Serra, M.-V. Density, Structure, and Dynamics of Water: The Effect of Van Der Waals Interactions. *J. Chem. Phys.* **2011**, *134*, 024516.

(18) Lin, I.-C.; Sietsonen, A. P.; Tavernelli, I.; Rothlisberger, U. Structure and Dynamics of Liquid Water from Ab Initio Molecular Dynamics-Comparison of BLYP, PBE, and RevPBE Density Functionals with and without Van Der Waals Corrections. *J. Chem. Theory Comput.* **2012**, *8*, 3902−3910.

(19) Zhang, Y.; Yang, W. Generalized Gradient Approximation Made Simple. *Phys. Rev. Lett.* **1998**, *80*, 890.

(20) Dion, M.; Rydberg, H.; Schröder, E.; Langreth, D. C.; Lundqvis, B. I. Van Der Waals Density Functional for General Geometries. *Phys. Rev. Lett.* **2004**, *92*, 246401.

(21) Zhang, C.; Wu, J.; Galli, G.; Gygi, F. Structural and Vibrational Properties of Liquid Water from Van Der Waals Density Functionals. *J. Chem. Theory Comput.* **2011**, *7*, 3054−3061.

(22) Perdew, J. P.; Yue, W. Accurate and Simple Density Functional for The Electronic Exchange Energy: Generalized Gradient Approximation. *Phys. Rev. B* **1986**, *33*, 8800. Murray, É. D.; Lee, K.; Langreth, D. C. Investigation of Exchange Energy Density Functional Accuracy for Interacting Molecules. *J. Chem. Theory Comput.* **2009**, *5*, 2754−2762.

(23) Klimes, J.; Bowler, D. R.; Michaelides, A. Chemical Accuracy for the Van Der Waals Density Functional. *J. Phys.: Condens. Matter* **2010**, *22*, 022201.

(24) Rey, R.; Møller, K. B.; Hynes, J. T. Hydrogen Bond Dynamics in Water and Ultrafast Infrared Spectroscopy. *J. Phys. Chem. A* **2002**, *106*, 11993−11996.

(25) Møller, K. B.; Rey, R.; Hynes, J. T. Hydrogen Bond Dynamics in Water and Ultrafast Infrared Spectroscopy: A Theoretical Study. *J. Phys. Chem. A* **2004**, *108*, 1275−1289.

(26) Schimdt, J. R.; Roberts, S. T.; Lopero, J. J.; Tokmakoff, A.; Fayer, M. D.; Skinner, J. L. Are Water Simulation Models Consistent with Steady-State and Ultrafast Vibrational Spectroscopy Experiments? *Chem. Phys.* **2007**, *341*, 143−157.

(27) Auer, B.; Kumar, R.; Schimdt, J. R.; Skinner, J. L. Hydrogen Bonding and Raman, IR, and 2D-IR Spectroscopy of Dilute HOD in Liquid D_2O. *Proc. Natl. Acad. Sci. U.S.A.* **2007**, *104*, 14215−14220.

(28) Lin, Y. S.; Auer, B. M.; Skinner, J. L. Water Structure, Dynamics, and Vibrational Spectroscopy in Sodium Bromide Solutions. *J. Chem. Phys.* **2009**, *131*, 144511.

(29) Skinner, J. L.; Auer, B. M.; Lin, Y. S. Vibrational Line Shapes, Spectral Diffusion, and Hydrogen Bonding in Liquid Water. *Adv. Chem. Phys.* **2009**, *142*, 59.

(30) Mallik, B. S.; Semparithi, A.; Chandra, A. Vibrational Spectral Diffusion and Hydrogen Bond Dynamics in Heavy Water from First Principles. *J. Phys. Chem. A* **2008**, *112*, 5104−5112.
(31) Mallik, B. S.; Semparithi, A.; Chandra, A. A First Principles Theoretical Study of Vibrational Spectral Diffusion and Hydrogen Bond Dynamics in Aqueous Ionic Solutions: D2O in Hydration Shells of Cl- Ions. *J. Chem. Phys.* **2008**, *129*, 194512.
(32) Fecko, C. J.; Eaves, J. D.; Loparo, J. J.; Tokamkoff, A.; Geissler, P. L. Ultrafast Hydrogen-Bond Dynamics in the Infrared Spectroscopy of Water. *Science* **2003**, *301*, 1698−1702.
(33) Omta, A. W.; Kropman, M. F.; Woutersen, S.; Bakker, H. J. Negligible Effect of Ions On the Hydrogen-Bond Structure in Liquid Water. *Science* **2003**, *301*, 347−349.
(34) Kropman, M. F.; Bakker, H. J. Dynamics of Water Molecules in Aqueous Solvation Shells. *Science* **2001**, *291*, 2118−2120.
(35) Kropman, M. F.; Bakker, H. J. Femtosecond Mid-Infrared Spectroscopy of Aqueous Solvation Shells. *J. Chem. Phys.* **2001**, *115*, 8942−8948.
(36) Park, S.; Fayer, M. D. Hydrogen Bond Dynamics in Aqueous NaBr Solutions. *Proc. Natl. Acad. Sci. U.S.A.* **2007**, *104*, 16731−16738.
(37) Bakker, H. J.; Kropman, M. F.; Omta, A. W.; Woutersen, S. Hydrogen-Bond Dynamics of Water in Ionic Solutions. *Phys. Scr.* **2004**, *69*, C14−24.
(38) Bakker, H. J. Structural Dynamics of Aqueous Salt Solutions. *Chem. Rev.* **2008**, *108*, 1456−1473.
(39) Nigro, B.; Re, S.; Laage, D.; Rey, R.; Hynes, J. T. On the Ultrafast Infrared Spectroscopy of Anion Hydration Shell Hydrogen Bond Dynamics. *J. Phys. Chem. A* **2006**, *110*, 11237−11243.
(40) Corcelli, S. A.; Lawrence, C. P.; Skinner, J. L. Combined Electronic Structure/Molecular Dynamics Approach for Ultrafast Infrared Spectroscopy of Dilute HOD in Liquid H_2O and D_2O. *J. Chem. Phys.* **2004**, *120*, 8107−8117.
(41) Corcelli, S. A.; Lawrence, C. P.; Asbury, J. B.; Steinel, T.; Fayer, M. D.; Skinner, J. L. Spectral Diffusion in a Fluctuating Charge Model of Water. *J. Chem. Phys.* **2004**, *121*, 8897−8900.
(42) Heisler, I. A.; Meech, S. R. Low-Frequency Modes of Aqueous Alkali Halide Solutions: Glimpsing the Hydrogen Bonding Vibration. *Science* **2010**, *327*, 857−860.
(43) Skinner, J. L. Following the Motions of Water Molecules in Aqueous Solutions. *Science* **2010**, *328*, 985−986.
(44) Smith, J. D.; Saykally, R. J.; Geissler, P. L. the Effects of Dissolved Halide Anions On Hydrogen Bonding in Liquid Water. *J. Am. Chem. Soc.* **2007**, *129*, 13847−13856.
(45) Thomas, A. S.; Elcock, A. H. Molecular Dynamics Simulations of Hydrophobic Associations in Aqueous Salt Solutions Indicate a Connection Between Water Hydrogen Bonding and the Hofmeister Effect. *J. Am. Chem. Soc.* **2007**, *129*, 14887−14898.
(46) Cappa, C. D.; Smith, J. D.; Messer, B. M.; Cohen, R. C.; Saykally, R. J. Effects of Cations On the Hydrogen Bond Network of Liquid Water: New Results from X-Ray Absorption Spectroscopy of Liquid Microjets. *J. Phys. Chem. B* **2006**, *110*, 5301−5309.
(47) Guardia, E.; Laria, D.; Marti, J. Hydrogen Bond Structure and Dynamics in Aqueous Electrolytes At Ambient and Supercritical Conditions. *J. Phys. Chem. B* **2006**, *110*, 6332−6338.
(48) Park, S.; Odelius, M.; Gaffney, K. J. Ultrafast Dynamics of Hydrogen Bond Exchange in Aqueous Ionic Solutions. *J. Phys. Chem. B* **2009**, *113*, 7825−7835.
(49) Nibbering, E. T. J.; Elsaesser, T. Ultrafast Vibrational Dynamics of Hydrogen Bonds in the Condensed Phase. *Chem. Rev.* **2004**, *104*, 1887−1914.
(50) Asbury, J. B.; Steinenl, T.; Stromberg, C.; Corcelli, S. A.; Lawrence, C. P.; Skinner, J. L.; Fayer, M. D. Water Dynamics: Vibrational Echo Correlation Spectroscopy and Comparison to Molecular Dynamics Simulations. *J. Phys. Chem. A* **2004**, *108*, 1107−1119.
(51) Laenen, R.; Rauscher, C.; Laubereau, A. Dynamics of Local Substructures in Water Observed By Ultrafast Infrared Hole Burning. *Phys. Rev. Lett.* **1998**, *80*, 2622. Laenen, R.; Simeonidis, K.; Laubereau, A. Subpicosecond Spectroscopy of Liquid Water in the Infrared: Effect of Deuteration on the Structural and Vibrational Dynamics. *J. Phys. Chem. B* **2002**, *106*, 408−417.
(52) Woutersen, S.; Emmerichs, U.; Bakker, H. J. Femtosecond Mid-IR Pump-Probe Spectroscopy of Liquid Water: Evidence for a Two-Component Structure. *Science* **1997**, *278*, 658−660. Woutersen, S.; Bakker, H. J. Hydrogen Bond in Liquid Water as a Brownian Oscillator. *Phys. Rev. Lett.* **1999**, *83*, 2077.
(53) Gale, G. M.; Gallot, G.; Hache, F.; Lascoux, N.; Bratos, S. Femtosecond Dynamics of Hydrogen Bonds in Liquid Water: a Real Time Study. *Phys. Rev. Lett.* **1999**, *82*, 1068. Bratos, S.; Gale, G. M.; Gallot, G.; Hache, F.; Lascoux, N.; Leickman, J.-C. Motion of Hydrogen Bonds in Diluted HDO/D_2O Solutions: Direct Probing with 150 Fs Resolution. *Phys. Rev. E* **2000**, *61*, 5211.
(54) Wang, Z.; Pakoulev, A.; Pang, Y.; Dlott, D. D. Vibrational Substructure in The OH Stretching Band of Water. *Chem. Phys. Lett.* **2003**, *378*, 281−288. Pakoulev, A.; Wang, Z.; Pang, Y.; Dlott, D. D. Vibrational Relaxation and Spectral Evolution Following Ultrafast OH Stretch Excitation of Water. *Chem. Phys. Lett.* **2001**, *371*, 594−600.
(55) Steinel, T.; Asbury, J. B.; Corcelli, S. A.; Lawrence, C. P.; Skinner, J. L.; Fayer, M. D. Water Dynamics: Dependence On Local Structure Probed with Vibrational Echo Correlation Spectroscopy. *Chem. Phys. Lett.* **2004**, *386*, 295−300.
(56) Asbury, J. B.; Steinel, T.; Kwak, K.; Corcelli, S. A.; Lawrence, C. P.; Skinner, J. L.; Fayer, M. D. Dynamics of Water Probed with Vibrational Echo Correlation Spectroscopy. *J. Chem. Phys.* **2004**, *121*, 12431−12446.
(57) Eaves, J. D.; Loparo, J. J.; Fecko, C. J.; Roberts, S. T.; Tokmakoff, A.; Geissler, P. L. Hydrogen Bonds in Liquid Water Are Broken Only Fleetingly. *Proc. Natl. Acad. Sci. U.S.A* **2005**, *102*, 13019−13022.
(58) Fecko, C. J.; Loparo, J. J.; Roberts, S. T.; Tokmakoff, A. Local Hydrogen Bonding Dynamics and Collective Reorganization in Water: Ultrafast Infrared Spectroscopy of HOD/D_2O. *J. Chem. Phys.* **2005**, *122*, 054506. Roberts, S. T.; Loparo, J. J.; Tokmakoff, A. Characterization of Spectral Diffusion from Two-Dimensional Line Shapes. *J. Chem. Phys.* **2006**, *125*, 084502.
(59) Eaves, J. D.; Tokmakoff, A.; Geissler, P. L. Electric Field Fluctuations Drive Vibrational Dephasing in Water. *J. Phys. Chem. A* **2005**, *109*, 9424−9436.
(60) Loparo, J. J.; Roberts, S. T.; Tokmakoff, A. Multidimensional Infrared Spectroscopy of Water. I. Vibrational Dynamics in Two-Dimensional IR Line Shapes. *J. Chem. Phys.* **2006**, *125*, 194521.
(61) Loparo, J. J.; Roberts, S. T.; Tokmakoff, A. Multidimensional Infrared Spectroscopy of Water. II. Hydrogen Bond Switching Dynamics. *J. Chem. Phys.* **2006**, *125*, 194522.
(62) Stenger, J.; Madsen, D.; Hamm, P.; Nibbering, E. T.; Elsaesser, T. A Photon Echo Peak Shift Study of Liquid Water. *J. Phys. Chem. A* **2002**, *106*, 2341−2350.
(63) Cowan, M. L.; Bruner, B. D.; Huse, N.; Dwyer, J. R.; Chugh, B.; Nibbering, E. T. J.; Elsaesser, T.; Miller, R. J. D. Ultrafast Memory Loss and Energy Redistribution in the Hydrogen Bond Network of Liquid H_2O. *Nature (London)* **2005**, *434*, 199−202.
(64) http://cp2k.berlios.de/.
(65) VandeVondele, J.; Krack, M.; Mohamed, F.; Parrinello, M.; Chassaing, T.; Hutter, J. Quickstep: Fast and Accurate Density Functional Calculations Using a Mixed Gaussian and Plane Waves Approach. *Comput. Phys. Commun.* **2005**, *167*, 103−128.
(66) Kohn, W.; Sham, L. Self-Consistent Equations Including Exchange and Correlation Effects. *J. Phys. Rev.* **1965**, *140*, A1133.
(67) VandeVondele, J.; Mohamed, F.; Krack, M.; Hutter, J.; Sprik, M.; Parrinello, M. the Influence of Temperature and Density Functional Models in Ab Initio Molecular Dynamics Simulation of Liquid Water. *J. Chem. Phys.* **2005**, *22*, 014515.
(68) Goedecker, S.; Teter, M.; Hutter, J. Separable Dual-Space Gaussian Pseudopotentials. *Phys. Rev. B* **1996**, *54*, 1703.
(69) Hartwigsen, C.; Goedecker, S.; Hutter, J. Relativistic Separable Dual-Space Gaussian Pseudopotentials from H to Rn. *Phys. Rev. B* **1998**, *58*, 3641.

(70) Nosé, S. a Molecular Dynamics Method for Simulations in the Canonical Ensemble. *Mol. Phys.* **1984**, *52*, 255−268. Hoover, W. G. Canonical Dynamics: Equilibrium Phase-Space Distributions. *Phys. Rev. A* **1985**, *31*, 1695.
(71) Martyna, G. J.; Klein, M. L.; Tuckerman, M. Nosé–Hoover Chains: The Canonical Ensemble Via Continuous Dynamics. *J. Chem. Phys.* **1992**, *97*, 2635−2643.
(72) Fuentes, M.; Guttorp, P.; Sampson, P. D. In *Statistical Methods For Spatio-Temporal Systems*; Finkenstadt, B., Held, L., Isham, V., Eds.; Chapman and Hall/CRC: London/Boca Raton, 2007; Chapter 3.
(73) Vela-Arevalo, L. V.; Wiggins, S. Time-Frequency Analysis of Classical Trajectories of Polyatomic Molecules. *Int. J. Bifurcation Chaos Appl. Sci. Eng.* **2001**, *11*, 1359−1380.
(74) Semparithi, A.; Keshavamurthy, S. Intramolecular Vibrational Energy Redistribution in DCO (X [Combining Tilde] 2 A): Classical-Quantum Correspondence, Dynamical Assignments of Highly Excited States, and Phase Space Transport. *Phys. Chem. Chem. Phys.* **2003**, *5*, 5051−5062 See Sec. IV for a Calculation of Time Dependent Frequencies Using the Wavelet Method..
(75) Soper, A. K. the Radial Distribution Functions of Water and Ice from 220 to 673 K and At Pressures Up to 400 MPa. *Chem. Phys.* **2000**, *258*, 121−137.
(76) Skinner, L. B.; Huang, C.; Schlesinger, D.; Pettersson, L. G. M.; Nilsson, A.; Benmore, C. J. Benchmark Oxygen-Oxygen Pair-Distribution Function of Ambient Water From X-Ray Diffraction Measurements with a Wide Q-Range. *J. Chem. Phys.* **2013**, *138*, 074506.
(77) McGrath, M. J.; Siepmann, J. I.; Kuo, I-F. W.; Mundy, C. J.; VandeVondele, J.; Hutter, J.; Mohamed, F.; Krack, M. IsobaricIso-thermal Monte Carlo Simulations From First Principles: Application to Liquid Water At Ambient Conditions. *ChemPhysChem* **2005**, *6*, 1439.
(78) Del Ben, M.; Schonherr, M.; Hutter, J.; VandeVondele, J. Bulk Liquid Water At Ambient Temperature and Pressure From MP2 Theory. *J. Phys. Chem. Lett.* **2013**, *4*, 3753.
(79) Marzari, N.; Vanderbilt, D. Maximally Localized Generalized Wannier Functions for Composite Energy Bands. *Phys. Rev. B* **1997**, *56*, 12847.
(80) Rapaport, D. Hydrogen Bonds in Water: Network Organization and Lifetimes. *Mol. Phys.* **1983**, *50*, 1151−1162.
(81) Balasubramanian, S.; Pal, S.; Bagchi, S. Hydrogen-Bond Dynamics Near a Micellar Surface: Origin of The Universal Slow Relaxation At Complex Aqueous Interfaces. *Phys. Rev. Lett.* **2002**, *89*, 115505.
(82) Luzar, A. Resolving The Hydrogen Bond Dynamics Conundrum. *J. Chem. Phys.* **2000**, *113*, 10663.
(83) Luzar, A.; Chandler, D. Effect of Environment On Hydrogen Bond Dynamics in Liquid Water. *Phys. Rev. Lett.* **1996**, *76*, 928. Luzar, A.; Chandler, D. Hydrogen-Bond Kinetics in Liquid Water. *Nature (London)* **1996**, *379*, 55−57.
(84) Chandra, A. Effects of Ion Atmosphere On Hydrogen-Bond Dynamics in Aqueous Electrolyte Solutions. *Phys. Rev. Lett.* **2000**, *85*, 768.
(85) Mills, R. Self-Diffusion in Normal and Heavy Water in The Range 1−45. Deg. *J. Phys. Chem.* **1973**, *77*, 685−688.
(86) Hardy, E. H.; Zygar, A.; Zeidler, M. D.; Holz, M.; Sacher, F. D. Isotope Effect On The Translational and Rotational Motion in Liquid Water and Ammonia. *J. Chem. Phys.* **2001**, *114*, 3174−3181.
(87) Samson, M. S. P.; Kerr, I. D.; Breed, J.; Sankararamakrishnan, R. Water in Channel-Like Cavities: Structure and Dynamics. *Biophys. J.* **1996**, *70*, 693−702.